MOLECULAR AND CELLULAR BIOLOGY, Mar. 2006, p. 2044–2054 Vol. 26, No. 6
0270-7306/06/$08.00+0 doi:10.1128/MCB.26.6.2044–2054.2006

Tankyrase 2 Poly(ADP-Ribose) Polymerase Domain-Deleted Mice Exhibit Growth Defects but Have Normal Telomere Length and Capping

Susan J. Hsiao,[1] Marc F. Poitras,[1] Brandoch D. Cook,[1] Yie Liu,[2] and Susan Smith[1]*

Skirball Institute of Biomolecular Medicine, New York University School of Medicine, 540 First Avenue, New York, New York 10016,[1] *and Oak Ridge National Laboratory, Life Sciences Division, Oak Ridge, Tennessee 37831-6445*[2]

Received 16 November 2005/Returned for modification 21 December 2005/Accepted 26 December 2005

Regulation of telomere length maintenance and capping are a critical cell functions in both normal and tumor cells. Tankyrase 2 (Tnks2) is a poly(ADP-ribose) polymerase (PARP) that has been shown to modify itself and TRF1, a telomere-binding protein. We show here by overexpression studies that tankyrase 2, like its closely related homolog tankyrase 1, can function as a positive regulator of telomere length in human cells, dependent on its catalytic PARP activity. To study the role of Tnks2 in vivo, we generated mice with the *Tnks2* PARP domain deleted. These mice are viable and fertile but display a growth retardation phenotype. Telomere analysis by quantitative fluorescence in situ hybridization (FISH), flow-FISH, and restriction fragment analysis showed no change in telomere length or telomere capping in these mice. To determine the requirement for Tnks2 in long-term maintenance of telomeres, we generated embryonic stem cells with the *Tnks2* PARP domain deleted and observed no change, even upon prolonged growth, in telomere length or telomere capping. Together, these results suggest that Tnks2 has a role in normal growth and development but is not essential for telomere length maintenance or telomere capping in mice.

Regulation of telomere length and protection of chromosome ends are two critical telomere functions that are essential in preventing premature senescence and in maintaining genome stability (reviewed in references 22 and 41). Mammalian telomeres consist of TTAGGG repeats that are bound by telomeric DNA repeat binding proteins and their associated factors, which together regulate telomere length maintenance and chromosome end protection (reviewed in references 17 and 56). TRF1, a double-stranded telomere repeat binding protein (12), functions as a negative regulator of telomere length by acting in *cis* to control access of telomerase (2, 58), a reverse transcriptase that uses an RNA template to add telomeric repeats (23, 24). Tankyrase 1 (Tnks1), which was identified in a two-hybrid screen with TRF1 (55), acts as a positive regulator of telomere length (54). Tankyrase 1 is comprised of several domains: the amino-terminal HPS domain, which consists of homopolymeric tracts of histidine, proline, and serine repeats; the large ANK domain, which is made up of 24 ankyrin repeats and comprises five functional subdomains (19, 50, 51); the sterile alpha module (SAM) domain, which is involved in tankyrase multimerization (18, 19, 50); and a poly(ADP-ribose) polymerase (PARP) domain (PD). The PARP domain of tankyrase 1 places this protein in the superfamily of PARP proteins.

PARPs utilize NAD^+ as a substrate to synthesize long linear or branched polymers of ADP-ribose on protein acceptors (reviewed in references 1 and 52). Tankyrase 1 poly(ADP-ribosyl)ates TRF1 in vitro, inhibiting its ability to bind to telomeric DNA (55). Upon overexpression of tankyrase 1 in the nucleus, TRF1 is removed from telomeres (13, 54). The DNA-unbound form of TRF1 is ubiquitinated and degraded by the proteasome (10). Long-term overexpression of tankyrase 1 in human cells results in loss of TRF1 and telomere elongation, dependent on the catalytic PARP activity of tankyrase 1 (13, 54).

Another function of tankyrase 1 was revealed by knockdown of tankyrase 1 expression. Tankyrase 1 short interfering RNA (siRNA) treatment in human cells resulted in mitotic arrest with aberrant chromosome configurations and abnormal spindle structures (20). Sister chromatids were able to separate at centromeres and arms but were unable to separate at their telomeres. Use of siRNA-resistant wild-type (WT), but not PARP-dead, tankyrase 1 rescued this phenotype, indicating a requirement for tankyrase 1 PARP activity in sister telomere resolution and mitotic progression (20). More recent studies characterized spindle defects in tankyrase 1 siRNA cells and found defects in bipolar spindle formation and supernumerary spindles (8).

In addition to its telomeric localization (via TRF1 binding), tankyrase 1 localizes to other subcellular sites, including mitotic centrosomes (53) and the Golgi apparatus (11), and has multiple binding partners. Tankyrase 1 has been shown to interact with IRAP (insulin-responsive aminopeptidase) in GLUT4 vesicles in the Golgi apparatus and further to be phosphorylated by mitogen-activated protein kinase upon insulin stimulation, suggesting a role for tankyrase 1 in mitogen-activated protein kinase-dependent regulation of GLUT4 vesicles (11). Tankyrase 1 has also been found to interact with and inhibit the Mcl-1 (myeloid cell leukemia 1) proteins, which function to regulate apoptosis (3). In addition, interactions of tankyrase 1 with FBP-17 (formin-binding protein 17) (21) and with TAB182 (tankyrase-binding protein of 182 kDa), a heterochromatin- and cortical actin-staining protein (51), have been observed. Finally, tankyrase 1 has been found to bind to

* Corresponding author. Mailing address: Skirball Institute of Biomolecular Medicine, New York University School of Medicine, 540 First Avenue, 2nd Floor, New York, NY 10016. Phone: (212) 263-2540. Fax: (212) 263-5711. E-mail: smithsu@saturn.med.nyu.edu.

and colocalize with NuMA (nuclear and mitotic apparatus protein) at mitotic centrosomes (49, 53). Recent studies indicate that NuMA is a major acceptor of poly(ADP-ribosyl)ation by tankyrase 1 in mitosis (8, 9).

Tankyrase 2 (Tnks2; a closely related homolog) was identified by several groups through two-hybrid screens with IRAP (11); Grb14, an SH2 domain-containing adaptor protein that binds to the insulin receptor (IR) (40); and TRF1 (29), as well as by serological screens using a fetal brain cDNA library with meningioma patient sera (42) or using a breast tumor cDNA library with breast carcinoma patient serum (36). Studies indicate that there is twofold more tankyrase 1 than tankyrase 2 in DT40 chicken cells (19). The domains that comprise tankyrase 2 are highly homologous to those of tankyrase 1, with the main exception being that tankyrase 2 lacks the HPS domain. The tankyrase 2 ANK domain shares 83% identity with that of tankyrase 1, and as the ANK domain is responsible for protein-protein interactions, tankyrase 2 interacts with many of the same proteins as tankyrase 1, including TRF1 (13, 29), TAB182 (51), NuMA (49), and IRAP (11, 50). The tankyrase 2 SAM domain shares 74% identity with that of tankyrase 1, allowing both self-oligomerization and oligomerization with tankyrase 1 (18, 19, 50). The PARP domain is the most conserved, with 94% identity. Tankyrase 2 has been shown to have PARP activity similar to that of tankyrase 1 (13, 50) and can poly(ADP-ribosyl)ate itself and TRF1, releasing TRF1 from telomeres (13).

To further elucidate the role of tankyrase 2 at telomeres, we generated stable human cell lines overexpressing tankyrase 2 in the nucleus. We show that tankyrase 2 induces telomere elongation, dependent on its catalytic PARP activity. Our results confirm that, as expected from the high degree of homology between the two proteins, tankyrase 2 (like tankyrase 1) can influence telomere length in human cells. Next, to study the function of tankyrase 2 on telomere length in vivo, we generated a tankyrase 2 PARP domain-deleted mouse. Characterization of this mouse revealed a small mouse phenotype, and telomere analysis showed no change in telomere length and no defect in telomere capping. Thus, in mice, a PARP-active Tnks2 is not required for telomere maintenance but is necessary for normal growth.

MATERIALS AND METHODS

Plasmids. Full-length tankyrase 2 (amino acids 2 to 1166) with an amino-terminal Myc tag and nuclear localization sequence (MN-TNKS2.WT) was cloned as described previously (13). MN-TNKS2.HE/A was generated by replacing the conserved active site histidine and glutamic acid residues at positions 1031 and 1138, respectively, with alanine residues by site-directed mutagenesis of MN-TNKS2.WT using oligonucleotides 5′-GCCAATGAACGAATGCTATTT GCTGGGTCTCCTTTTGTGAATG-3′ for H1031 and 5′-GGCCTAGCATTA GCTGCATATGTTATTTACAGAGGAGAAC-3′ for E1138, with the Stratagene QuickChange site-directed mutagenesis kit. MN-TNKS2.WT and MN-TNKS2.HE/A were cloned into the pLPC vector, and HTC75 retroviral cell lines were generated as previously described (13).

Cell lines. Mouse embryo fibroblasts (MEFs) were generated from embryos isolated at embryonic day 13.5 from $Tnks2^{PD\Delta}$ or $Tnks2^{PD\Delta neo\Delta}$ mice (see "Generation of *Tnks2* mutant mice") and were cultured in Dulbecco modified Eagle medium (DMEM)-10% fetal bovine serum (FBS) (HyClone). MEFs were immortalized using the 3T3 protocol (57). $Tnks2^{PD\Delta-/-}$ embryonic stem (ES) cells were generated from G418-resistant $Tnks2^{PD\Delta+/-}$ ES cells (see below for description) by selection at increased G418 concentration (500 μg/ml). Two independent clones (A3 and C10) were isolated. ES cells were cultured on gelatinized plates at 37°C, 6.5% CO_2 in DMEM–15% heat-inactivated FBS (HyClone)–1 mM sodium pyruvate–10^{-4} M β-mercaptoethanol–1,000 U/ml leukemia inhibitory factor (Chemicon).

Antibody generation. Anti-tankyrase 2 antibody 608 was raised and affinity purified against an *Escherichia coli*-expressed fusion protein containing human tankyrase 2 amino acids 811 to 896.

Immunoblotting and immunoprecipitation. Twenty-five micrograms of cell or tissue extracts, prepared as described previously (13), or baculovirus-derived tankyrase 1 (55) or tankyrase 2 (13) proteins was fractionated by sodium dodecyl sulfate-polyacrylamide gel electrophoresis and was transferred to a nitrocellulose membrane. Blots were incubated with the following primary antibodies: rabbit anti-Myc (0.8 μg/ml; Santa Cruz Biotechnology), rabbit anti-TRF1 415 (0.5 μg/ml) (13), rabbit anti-tankyrase 2 608 (0.7 μg/ml), rabbit anti-β-actin (0.2 μg/ml; Santa Cruz Biotechnology), and rabbit anti-tankyrase 1 465 (1.8 μg/ml) (55). Immunoprecipitation of cell or tissue extracts was performed as described previously (13) using 1.8 μg/ml rabbit anti-tankyrase 1 465.

Construction of *mTnks2* targeting vector. The targeting vector was designed to replace exons 25, 26, and 27 (PARP domain of Tnks2) with a neomycin (*neo*) resistance cassette. (Note that the *mTnks2* exon nomenclature that is used in this paper follows that described in reference 29. The predicted exon structure for *mTnks2* in the GenBank and Mouse Genome Informatics databases includes one additional exon upstream of exon 1.) The floxed phosphoglycerate kinase-*neo* cassette from the pPNTloxPneo vector (kindly provided by Alexandra Joyner, Skirball Institute) was cloned into pSP72 (from Promega, with a NotI site added to the P6 site). The 1.5-kb short arm was generated by PCR from mouse 129/SvEv genomic DNA using primers 5′-GTGGGAAAGATATACACACCG GAG-3′ and 5′-GTGCACATCAGTCAAGCACTGAG-3′. The short arm began within exon 24 and extended to 90 bp upstream of exon 25 and was inserted 5′ of the *neo* cassette. The long arm, which began at the XbaI site downstream of exon 27 and extended 7.5 kb, was generated from a λ phage clone isolated from a mouse 129/SvEv genomic library and was inserted 3′ of the *neo* cassette.

Targeted disruption of the *mTnks2* gene in ES cells. Ten micrograms of the targeting vector was linearized with NotI and electroporated into 129/SvEv ES cells. After selection in G418 (200 μg/ml), surviving colonies were expanded, and PCR analysis was performed to identify clones that had undergone homologous recombination. To detect the wild-type allele, the following primer pair was used: primer 1, 5′-GTGGGAAAGATATACACACCGGAG-3′, and primer 2, 5′-AAA TTCCAGCTCCAAACATGCCAC-3′. For the mutant allele, the following primer pair was used: primer 3, 5′-GACAACTTACGGCAGTTGGTTCTG-3′, and primer 4, 5′-TGCGAGGCCAGAGGCCACTTGTGTAGC-3′. The PCR conditions were 94°C for 5 min; followed by 35 cycles of 94°C for 30 s, 62°C for 1 min, and 72°C for 2 min; and a final extension at 72°C for 7 min.

Generation of $Tnks2^{PD\Delta}$ mice. $Tnks2^{PD\Delta}$ heterozygous (+/−) ES cell clones were microinjected into C57BL/6 blastocysts, and chimeric males were mated to C57BL/6 females for germ line transmission of the targeted allele. Genotyping was performed using the PCR primers above, and correct targeting was confirmed by Southern blotting. Homologous recombination of the targeting vector with the *Tnks2* gene resulted in the introduction of a ScaI site, which was used to distinguish the 4.3-kb fragment in the wild-type allele from the 5.1-kb fragment in the mutant allele, by a 0.5-kb 5′-flanking probe. The probe was generated by PCR using the following primers: 5′-TTGTTCATACCAGCTATGGTT CTTG-3′ and 5′-GTGTCTGTCTGAGTTCATACAC-3′.

Generation of $Tnks2^{PD\Delta neo\Delta}$ mice. $Tnks2^{PD\Delta}$ null (−/−) mice were crossed to C57BL/6 mice carrying a thymidine kinase (TK)-*Cre* transgene (kindly provided by Alexandra Joyner, Skirball Institute [5]) to remove the floxed *neo* cassette. $Tnks2^{PD\Delta neo\Delta+/-}$ TK-*Cre* mice were backcrossed to C57BL/6 mice to remove the TK-*Cre* transgene. These $Tnks2^{PD\Delta neo\Delta+/-}$ mice were backcrossed again to C57BL/6 mice before breeding $Tnks2^{PD\Delta neo\Delta+/-}$ mice to generate $Tnks2^{PD\Delta neo\Delta-/-}$ mice. Genotyping was performed using PCR primers 1 and 2 (see above) for the wild-type allele and primers 1 and 5 for the mutant, *neo*-deleted allele, using the same PCR conditions as used above (PCR primer 5, 5′-GAGTTCAGAAGCTGGGGCTTA GCATC-3′). Southern blotting was performed using the probe described above.

Mouse breeding and housing. $Tnks2^{PD\Delta}$ mice were maintained on a mixed 129/SvEv-C57BL/6 background; $Tnks2^{PD\Delta neo\Delta}$ mice were backcrossed twice to C57BL/6 mice. Mice were housed in a specific-pathogen-free facility, in accordance with institutional animal care guidelines.

Northern blotting. Total RNA was prepared from MEFs using the RNeasy Mini kit (QIAGEN). Blots were probed with DNA probes corresponding to amino acids 811 to 896 for human tankyrase 2 and 336 to 1163 for human tankyrase 1.

Telomere restriction fragment analysis. Genomic DNA was isolated from stable HTC75 cell lines expressing vector, MN-TNKS2.WT or MN-TNKS2.HE/A, and digested with HinfI and RsaI. Telomere restriction fragments were detected by Southern blotting with a ^{32}P-labeled TTAGGG probe, as previously described

(13). The mean length of telomeric restriction fragments was determined using TELO software (Fox Chase Cancer Center). For primary or immortalized MEFs of the indicated genotypes, cells were embedded in agarose plugs and digested with HinfI and RsaI, DNA fragments were separated by pulsed-field gel electrophoresis (CHEF DR-II apparatus, Bio-Rad), and telomere restriction fragments were analyzed, as described previously (20).

Quantitative fluorescence in situ hybridization (Q-FISH). Spleens from wild-type and *Tnks2*$^{PD\Delta}$ littermate mice, or wild-type and *Tnks2*$^{PD\Delta neo\Delta}$ littermate mice, were used to prepare single-cell suspensions by mincing samples through a 70-μm nylon cell strainer (BD Biosciences). Splenocytes were cultured in DMEM-10% FBS and activated with 1 μg/ml concanavalin A (Sigma) and 1 μg/ml phytohemagglutinin (Sigma) for 36 h before cells were arrested in metaphase with a 6-h treatment with 0.1 μg/ml Colcemid (Gibco). Cells were collected, and metaphase spreads were prepared from splenocytes as described previously (20) and from ES cells as described previously (61). Images were acquired on a Zeiss Axioplan 2 microscope with a Photometrix SenSyn camera. Photographs were processed using OpenLab software. TFL-TELO software (kindly provided by P. Lansdorp, Terry Fox Laboratory, Vancouver, Canada) was used to quantify the telomere signal from 10 metaphases for each sample.

Flow-FISH. Spleen and thymus from wild-type and *Tnks2*$^{PD\Delta}$ littermate mice or wild-type and *Tnks2*$^{PD\Delta neo\Delta}$ littermate mice were used to prepare single-cell suspensions of splenocytes and thymocytes by mincing samples through a 70-μm nylon cell strainer. Erythrocytes were removed from the cell suspension by lysis with ACK lysing buffer, and samples were frozen at −80°C until processed for flow-FISH. Frozen samples were thawed and washed two times in DMEM. Viable cells were counted and resuspended in phosphate-buffered saline–0.1% bovine serum albumin (BSA) to the concentration of 1×10^6 cells/ml. Cells were pelleted and resuspended in 1 ml of hybridization solution [70% formamide, 20 mM Tris, pH 7.5, 20 mM NaCl, 1% BSA, 0.3 μg/ml fluorescein isothiocyanate-conjugated $(TTAGGG)_3$ peptide nucleic acid (PNA) probe (Applied Biosystems)]. DNA was denatured at 86°C for 10 min, and the samples were hybridized for 2 h at room temperature. Cells were washed four times in wash solution 1 (70% formamide, 10 mM Tris, pH 7.5, 1% BSA, 1% Tween 20) and one time in wash solution 2 (5% glucose, 10 mM HEPES, 1% BSA, 1% Tween 20). For DNA counterstaining, cells were resuspended in 500 μl staining solution (phosphate-buffered saline, 10 U/ml RNase A, 0.1% BSA, 0.1 μg/ml propidium iodide) for 2 h before acquisition on the FACScan (Becton Dickinson) flow cytometer. Mean telomere fluorescence of cells gated at G_0/G_1 was analyzed with CellQuest software.

Scoring of chromosomal abnormalities. The indicated number of metaphase images for each sample was scored for chromosomal abnormalities (end-to-end fusions, chromosome breakages, and signal free ends) by overlaying the telomere image on the chromosome image using Photoshop software.

RESULTS

Human tankyrase 2 is a positive regulator of telomere length. Previous studies indicated that tankyrase 2 shared a number of properties with tankyrase 1. Both were found to bind TRF1 and poly(ADP-ribosyl)ate TRF1 in vitro (13, 29, 55). Overexpression studies of tankyrase 1 showed that when it was expressed in the nucleus (via an amino-terminal nuclear localization signal) it removed TRF1 from telomeres (whereupon TRF1 was degraded by the proteasome) and, over the long term, induced telomerase-dependent telomere elongation (10, 13, 54). The activities of tankyrase 1 were dependent on its catalytic PARP domain, since a catalytically dead allele (tankyrase 1.HE/A) had no effect on TRF1 or telomere length maintenance (13). We showed previously that overexpression of a Myc epitope-tagged, nuclear localization signal-containing tankyrase 2 (MN-tankyrase 2) resulted in loss of TRF1 from telomeres (13). To determine if tankyrase 2 (like tankyrase 1) was capable of inducing telomere elongation, we generated stable HTC75 cell lines expressing MN-tankyrase 2 WT or a PARP-dead allele (HE/A) (generated in the same way as tankyrase 1.HE/A) by converting the highly conserved active site residues, histidine and glutamic acid at amino acid positions 1031 and 1138, respectively, to alanine residues by site-directed mutagenesis. As shown in Fig. 1A, overexpression of wild-type (lane 2) but not PARP-dead (lane 3) tankyrase 2 resulted in reduced levels of TRF1. Telomere length analysis showed that MN-tankyrase 2.WT induced telomere elongation (Fig. 1B). Telomeres showed progressive elongation at a rate of approximately 38 bp per population doubling (pd) (Fig. 1C), similar to tankyrase 1 (13, 54). By contrast, overexpression of MN-tankyrase 2.HE/A had no effect on telomere elongation (Fig. 1B and C) and was similar to a vector control (data not shown). Together these studies indicate that tankyrase 2 (like tankyrase 1) can act as a positive regulator of telomere length in human cells dependent on its catalytic PARP activity.

To determine if tankyrase 2 is required to maintain telomere length in vivo, we sought to delete the tankyrase 2 gene (*Tnks2*) in mouse. In order to monitor tankyrase 2 protein expression, we raised tankyrase 2-specific antibodies against an *E. coli*-expressed fusion protein containing human tankyrase 2 amino acids 811 to 896 (Fig. 1D). The specificity of the antibody was determined by immunoblotting against baculovirus-expressed human tankyrase 1 or tankyrase 2. As shown in Fig. 1E, anti-tankyrase 2 608 specifically detected tankyrase 2 (lane 4) but not tankyrase 1 (lane 3). By contrast, a previously generated antibody to tankyrase 1 (tankyrase 1 465) (55) detected both tankyrase 1 (lane 5) and tankyrase 2 (lane 6).

Generation of *Tnks2*$^{PD\Delta}$ and *Tnks2*$^{PD\Delta neo\Delta}$ mice. *Tnks2* is located on mouse chromosome 19qC2. The gene is comprised of 27 exons. (See note in Materials and Methods.) The last four exons (24 through 27) encode the carboxy-terminal catalytic PARP domain of tankyrase 2 (Fig. 2A). We sought to disrupt the *Tnks2* gene and create a null allele by deleting exons 25 through 27 (encoding carboxy-terminal amino acids 1032 through 1166 of *mTnks2*) and replacing them with the neomycin resistance gene (*neo*). However, as described below, the targeted disruption did not result in a null allele but rather in expression of truncated forms of Tnks2. The truncated proteins lack the catalytic PARP domain; hence, the targeted allele will be referred to as *Tnks2*$^{PD\Delta}$ (PARP domain deleted) (Fig. 2A).

Mouse ES cells (129/SvEv) were electroporated with the linearized targeting construct and selected for G418 resistance. Clones were screened using the PCR strategy described below. Chimeric mice (generated from injection of a positive ES cell clone into a blastocyst) were mated to C57BL/6 for germ line transmission to generate *Tnks2*$^{PD\Delta+/-}$ mice.

Mating of *Tnks2*$^{PD\Delta+/-}$ mice generated *Tnks2*$^{PD\Delta-/-}$ mice, as shown by Southern blotting and PCR analysis of tail DNA. For Southern blot analysis, to monitor the targeting of the *Tnks2* locus, we made use of a ScaI site in the *neo* gene, which generates a 5.1-kb ScaI fragment that can be distinguished from the 4.3-kb ScaI fragment in the wild-type allele (Fig. 2A and B). The genotype of the mice was further confirmed using PCR analysis (Fig. 2A and C). For the wild-type allele, PCR was performed with a 5′ primer in exon 24 and a 3′ primer in exon 25, which resulted in a 1.7-kb fragment specific to the wild-type allele. For the targeted allele PCR was performed with a 5′ primer upstream of exon 24 (not found in the targeting vector) and a 3′ primer in the *neo* gene, which resulted in a 2.0-kb fragment specific to the targeted allele.

Consistent with targeting of the *Tnks2* locus, Northern blot analysis of primary MEFs showed no detectable *Tnks2* RNA

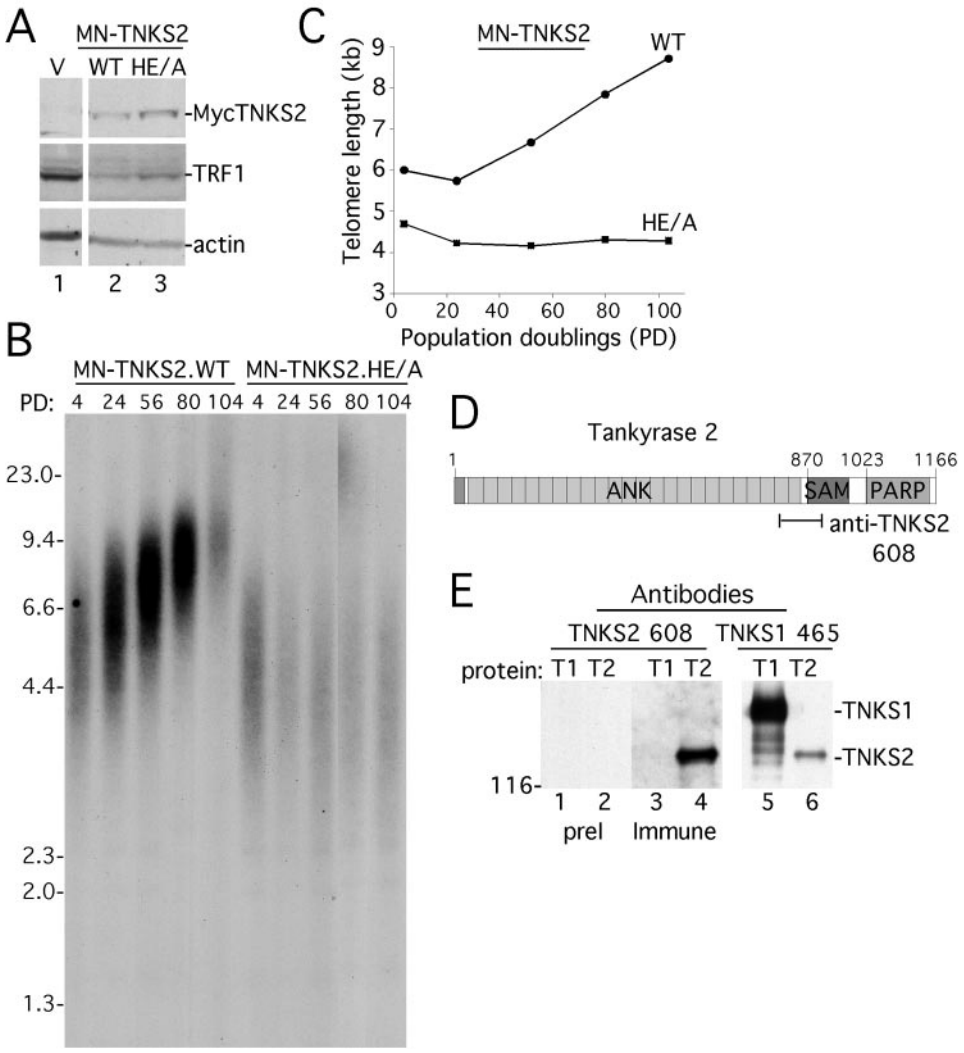

FIG. 1. Human tankyrase 2 promotes telomere elongation. (A) Immunoblot analysis of whole-cell extracts from stable HTC75 cell lines expressing a vector control (V) or MN-tankyrase 2 wild type (MN-TNKS2.WT) or MN-tankyrase 2 HE/A (MN-TNKS2.HE/A). Immunoblots were probed with anti-Myc, anti-TRF1, or anti-β-actin antibodies. (B) Southern blot analysis of HinfI/RsaI-digested genomic DNA from stable HTC75 cell lines expressing MN-TNKS2.WT or HE/A at the indicated pd. Telomere restriction fragments were detected with a ^{32}P-labeled TTAGGG repeat probe. (C) Graphical representation of telomere length changes in stable HTC75 cell lines expressing MN-TNKS2.WT or HE/A. Plots represent the mean telomere length values derived from the Southern blots in panel B. (D) Schematic diagram of human tankyrase 2. ANK, ankyrin repeat domain. The region against which anti-tankyrase 2 608 was raised is indicated by a line. (E) Immunoblot analysis demonstrating the specificity of anti-tankyrase 2 608. Partially purified baculovirus-derived tankyrase 1 (T1) or tankyrase 2 (T2) was fractionated by sodium dodecyl sulfate-polyacrylamide gel electrophoresis and analyzed by immunoblotting with preimmune (preI) serum, affinity-purified anti-tankyrase 2 608 (Immune), or anti-tankyrase 1 465. Numbers at left of panels B and E are molecular masses in kilobases and kilodaltons, respectively.

(Fig. 2D). Moreover, we did not detect any major new transcripts in *Tnks2*$^{PD\Delta+/-}$ or *Tnks2*$^{PD\Delta-/-}$ cells. As expected, immunoblot analysis of immortalized MEFs indicated that wild-type (full-length) Tnks2 was not expressed in *Tnks2*$^{PD\Delta-/-}$ cells (Fig. 2E). However, alternative Tnks2 proteins (which were not found in wild-type cells) were expressed in *Tnks2*$^{PD\Delta+/-}$ and *Tnks2*$^{PD\Delta-/-}$ cells, indicating that deletion of exons 25 through 27 did not result in complete ablation of Tnks2 protein expression. Our failure to detect alternative transcripts by Northern blotting could be due to their lower abundance or stability.

We observed two classes of alternative Tnks2 proteins in *Tnks2*$^{PD\Delta+/-}$ and *Tnks2*$^{PD\Delta-/-}$ cells, one migrating faster and the other slower than wild-type Tnks2 protein (Fig. 2E). The faster-migrating proteins likely corresponded to truncated Tnks2 proteins. The targeted *Tnks2* allele lacks the carboxy-terminal 134 amino acids. Thus, a truncated protein would be predicted to migrate with an apparent molecular mass of 114 kDa (compared to 128 kDa for wild-type Tnks2), consistent with the protein analysis in Fig. 2E. The truncated Tnks2 proteins likely contain the ANK and SAM domains, which are important for scaffolding functions and protein-protein interactions. However, the alternative Tnks2 proteins lack the catalytic PARP domain and are therefore PARP dead.

We reasoned that the slower-migrating class of proteins may have resulted from splicing of a truncated *Tnks2* to downstream sequences, in particular *neo*. Other groups have re-

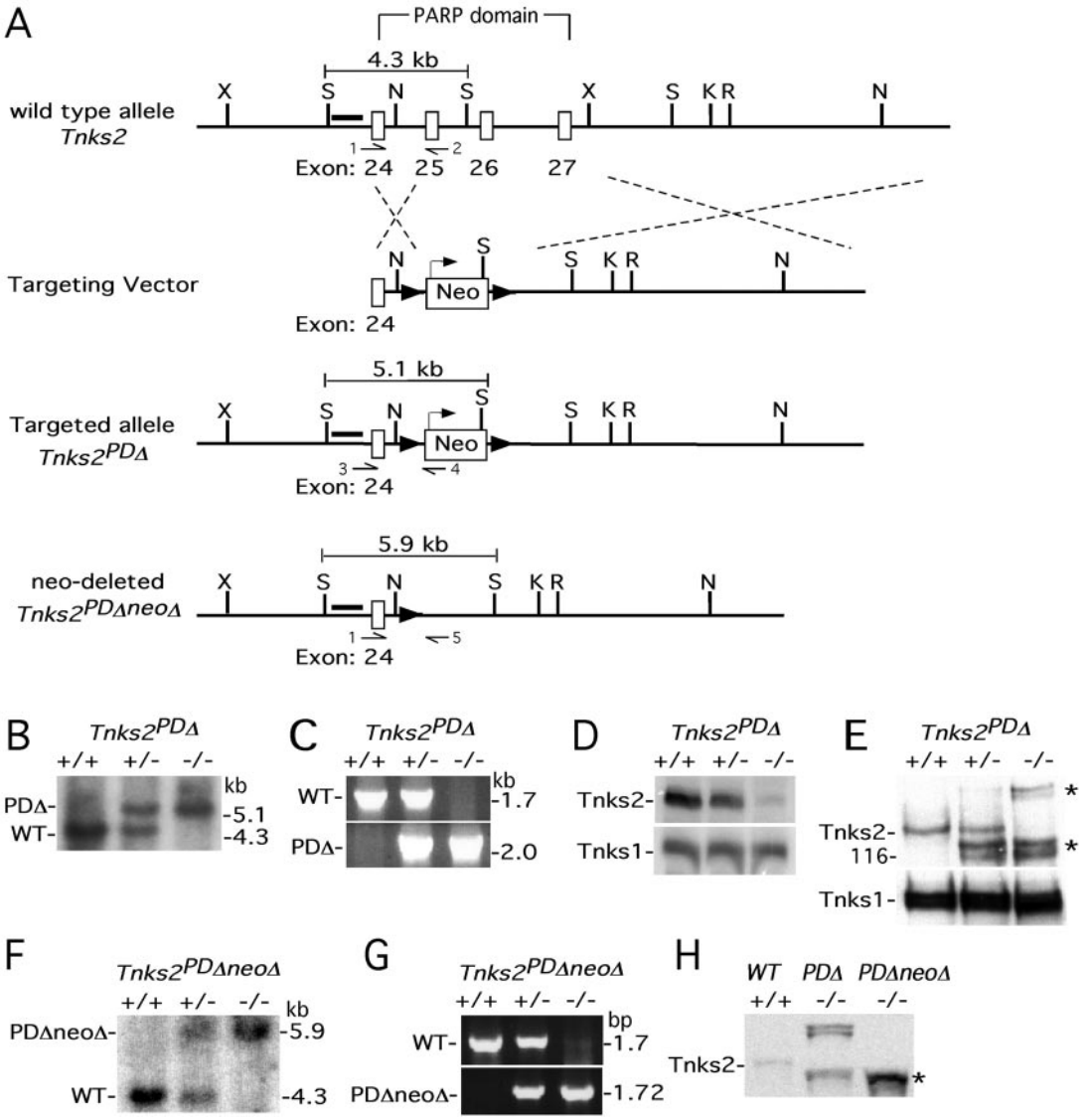

FIG. 2. Targeted deletion of exons 25, 26, and 27 (encoding the catalytic PARP domain) of mouse *Tnks2*. (A) Schematics of the wild-type allele, targeting construct, targeted allele, and the *neo*-deleted targeted allele (top to bottom lines, respectively). The 4.3-, 5.1-, and 5.9-kb ScaI fragments used for genotyping are indicated. Positions of PCR primers used for genotyping are indicated by half arrows. LoxP sites are indicated by arrowheads. Bar indicates the 0.5-kb probe 0.2 kb upstream of exon 24 used for Southern blotting. Restriction sites: X, XbaI; S, ScaI; N, NcoI; K, KpnI; R, EcoRI. (B to E) Characterization of $Tnks2^{PD\Delta}$. (B) Southern blot of ScaI-digested tail DNA from the indicated genotypes using the 0.5-kb probe indicated by a bar in panel A. (C) PCR analysis of mouse tail DNA of the indicated genotypes using the primers indicated in panel A. (D) Northern blot of total RNA from primary MEFs of the indicated genotypes. RNA was hybridized first with a radiolabeled tankyrase 2 probe and subsequently with a tankyrase 1 probe. (E) Immunoblot analysis of immortalized MEFs of the indicated genotypes. Cell extracts were immunoprecipitated with anti-tankyrase 1 465 (detects tankyrases 1 and 2) and immunoblotted with anti-tankyrase 2 608 or anti-tankyrase 1 465 antibodies. Asterisks indicate alternative products of Tnks2 lacking the catalytic PARP domain. (F to H) Characterization of $Tnks2^{PD\Delta neo\Delta}$. (F) Southern blot of ScaI-digested tail DNA of the indicated genotypes using the 0.5-kb probe indicated by the bar shown in panel A. (G) PCR analysis of mouse tail DNA of the indicated genotypes using the primers indicated in panel A. (H) Immunoblot analysis of brain extracts of the indicated genotypes. Brain extracts were immunoprecipitated with anti-tankyrase 1 465 (detects tankyrases 1 and 2) and immunoblotted with anti-tankyrase 2 608. The asterisks indicates an alternative product of Tnks2 lacking the catalytic PARP domain.

ported generating neo fusion proteins when attempting targeted gene disruption with the *neo* cassette and have noted the presence of cryptic splice sites within the cassette (7, 28). As the *neo* gene in the targeted allele was flanked by loxP sites (Fig. 2A), we addressed this possibility by deleting the *neo* gene from the targeted allele using Cre recombinase. Thus, we crossed $Tnks2^{PD\Delta-/-}$ mice to C57BL/6 mice carrying a TK-*Cre* transgene. The $Tnks2^{PD\Delta neo\Delta+/-}$ TK-*Cre* mice were backcrossed to C57BL/6 mice to remove TK-*Cre*. These $Tnks2^{PD\Delta neo\Delta+/-}$ mice were backcrossed again to C57BL/6 mice before breeding heterozygous mice to generate $Tnks2^{PD\Delta neo\Delta-/-}$ mice. To monitor excision of the *neo* allele, we took advantage of replacement of the ScaI site in the *neo* gene with a downstream ScaI site which resulted in a 5.9-kb ScaI fragment, distinguishing the *PDΔneoΔ* allele from the

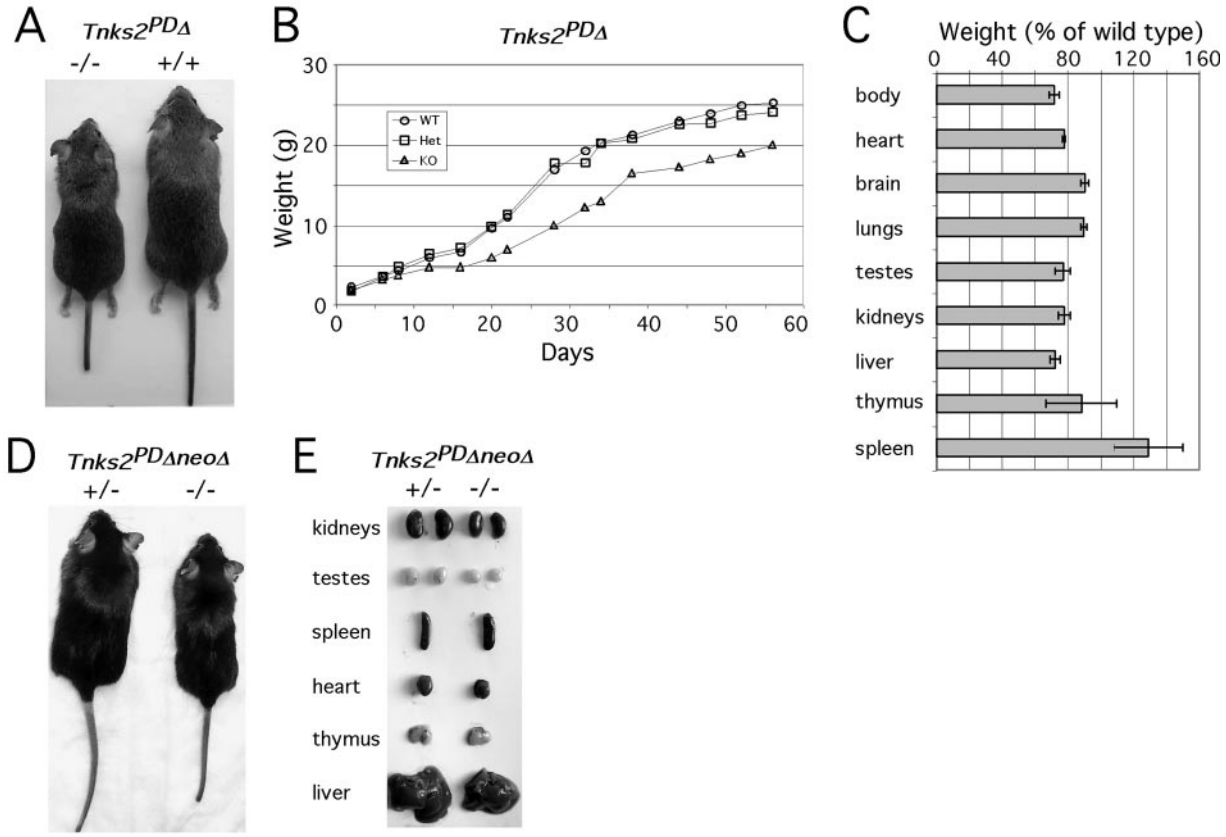

FIG. 3. Tnks2$^{PD\Delta-/-}$ and *Tnks2*$^{PD\Delta neo\Delta-/-}$ mice are smaller than heterozygous or wild-type mice. (A) Photograph of a representative *Tnks2*$^{PD\Delta-/-}$ mouse and wild-type littermate at 6 weeks of age. (B) Growth curve of male *Tnks2*$^{PD\Delta}$ mice. Graph shows the average weights of *Tnks2*$^{PD\Delta-/-}$ (four male), *Tnks2*$^{PD\Delta+/-}$ (five male), and *Tnks2*$^{PD\Delta+/+}$ (three male) mice taken on the day indicated (or the following day) for a period of 56 days. (C) Average organ weight (± standard error of the mean) of three *Tnks2*$^{PD\Delta-/-}$ mice compared to three *Tnks2*$^{PD\Delta+/+}$ mice taken at 6 to 7 weeks of age. (D and E) *Tnks2*$^{PD\Delta neo\Delta-/-}$ mice show the small mouse phenotype. (D) Photograph of a representative *Tnks2*$^{PD\Delta neo\Delta-/-}$ mouse and *Tnks2*$^{PD\Delta neo\Delta+/-}$ littermate at 6 weeks of age. (E) Macroscopic appearance of selected organs from a *Tnks2*$^{PD\Delta neo\Delta-/-}$ mouse and *Tnks2*$^{PD\Delta neo\Delta+/-}$ littermate at 6 weeks age.

wild-type allele (Fig. 2A and F). The genotype of the mice was further confirmed using PCR analysis (Fig. 2A and G). For the wild-type allele, PCR was performed (as described above) with a 5′ primer in exon 24 and a 3′ primer in exon 25, which resulted in a 1.7-kb fragment specific to the wild-type allele. For the *neo*-deleted allele PCR was performed with a 5′ primer upstream of exon 24 and a 3′ primer just 3′ to the remaining loxP site, which resulted in a 1.72-kb fragment specific to the *neo*-deleted allele. As shown by immunoblot analysis of brain tissue, the high-molecular-weight protein was no longer expressed in the *Tnks2*$^{PD\Delta neo\Delta-/-}$ mice; only the low-molecular-weight, truncated products remained (Fig. 2H).

Small size in *Tnks2*$^{PD\Delta-/-}$ and *Tnks2*$^{PD\Delta neo\Delta-/-}$ mice. As described above, mating of *Tnks2*$^{PD\Delta+/-}$ mice generated *Tnks2*$^{PD\Delta-/-}$ mice at the expected Mendelian ratio (37 *Tnks2*$^{PD\Delta-/-}$ mice, 69 *Tnks2*$^{PD\Delta+/-}$ mice, and 35 *Tnks2*$^{PD\Delta+/+}$ mice). *Tnks2*$^{PD\Delta-/-}$ mice (both male and female) were viable and fertile. However, a small but significant fraction died within 20 days of birth (7/37 [19%] *Tnks2*$^{PD\Delta-/-}$ mice, 1/69 [1%] *Tnks2*$^{PD\Delta+/-}$ mice, and 2/35 [6%] *Tnks2*$^{PD\Delta+/+}$ mice). The most striking feature of the *Tnks2*$^{PD\Delta-/-}$ mice was their smaller body size (Fig. 3A). We monitored the weight of the mice from birth to 8 weeks. As shown in Fig. 3B, *Tnks2*$^{PD\Delta-/-}$ pups showed a weight similar to that of their wild-type and *Tnks2*$^{PD\Delta+/-}$ littermates 2 and 4 days after birth. However, by 6 days *Tnks2*$^{PD\Delta-/-}$ pups weighed less than their littermates. The difference was most dramatic at 20 days (*Tnks2*$^{PD\Delta-/-}$ mice were 40% smaller than *Tnks2*$^{PD\Delta+/-}$ and *Tnks2*$^{PD\Delta+/+}$ mice) but decreased over time (at 56 days *Tnks2*$^{PD\Delta-/-}$ mice were 20% smaller than *Tnks2*$^{PD\Delta+/-}$ and *Tnks2*$^{PD\Delta+/+}$ mice). The weights of heart, brain, lungs, testis, kidneys, and liver were proportionately reduced in size, but thymus and spleen were variable (Fig. 3C). We also observed a few cases of severely small *Tnks2*$^{PD\Delta-/-}$ mice that were 50 to 60% smaller than *Tnks2*$^{PD\Delta+/-}$ and *Tnks2*$^{PD\Delta+/+}$ mice; however, these mice tended to die before weaning and were not included in the growth curve or organ size analysis.

Tnks2$^{PD\Delta neo\Delta-/-}$ mice exhibited a similar small mouse phenotype (Fig. 3D and E), indicating that the phenotype was consistent in both the *Tnks2*$^{PD\Delta-/-}$ and *Tnks2*$^{PD\Delta neo\Delta-/-}$ mice. However, compared to the *Tnks2*$^{PD\Delta}$ mice, we noticed an increase in death before 20 days of age in both *Tnks2*$^{PD\Delta neo\Delta+/-}$ and *Tnks2*$^{PD\Delta neo\Delta-/-}$ mice (6/33 [18%] *Tnks2*$^{PD\Delta neo\Delta+/-}$ mice and 11/20 [55%] *Tnks2*$^{PD\Delta neo\Delta-/-}$ mice) and an approximately twofold increase (data not shown) in the number of severely

TABLE 1. Measurement by flow-FISH of telomere length in splenocytes and thymocytes obtained from *Tnks2*$^{PD\Delta}$ (−/−) and *Tnks2*$^{PD\Delta neo\Delta}$ (−/−) mice and their wild-type (+/+) or heterozygous (+/−) littermates

Mouse type	Litter	Mouse no.[a]	Genotype	Telomere length[b]	
				Spleen	Thymus
Tnks2$^{PD\Delta}$	1	M395	+/+	1.44	0.93
		M396	−/−	1.42	1.04
		F397	+/+	1.63	0.80
		F399	+/+	0.67	1.07
		F401	−/−	0.96	0.97
		F402	−/−	1.53	0.59
	2	M443	+/+	0.53	0.98
		M446	−/−	0.62	1.37
		F448	−/−	0.96	1.74
		F450	+/+	0.99	0.84
	3	F467	+/+	0.56	0.66
		F468	−/−	0.83	1.04
Tnks2$^{PD\Delta neo\Delta}$	1	F502	+/+	0.77	0.88
		F501	−/−	1.01	1.06
	2	F559	+/+	1.60	1.26
		F560	−/−	1.08	1.05
	3	M628	+/−	0.95	0.87
		M629	−/−	0.82	0.98
	4	F600	+/−	1.28	0.95
		F601	−/−	0.92	0.82
		F602	−/−	0.98	0.83
		F604	+/−	0.79	1.15

[a] M, male; F, female.

[b] Telomere length is expressed in arbitrary fluorescent units. For *Tnks2*$^{PD\Delta}$ mice, average telomere fluorescence was 0.88 (+/+) versus 1.13 (−/−) in splenocytes ($P = 0.19$) and 0.97 (+/+) versus 1.05 (−/−) in thymocytes ($P = 0.29$). For *Tnks2*$^{PD\Delta neo\Delta}$ mice, average telomere fluorescence was 1.07 (+/+ or +/−) versus 0.94 (−/−) in splenocytes ($P = 0.42$) and 1.03 (+/+ or +/−) versus 0.97 (−/−) in thymocytes ($P = 0.57$).

small *Tnks2*$^{PD\Delta neo\Delta-/-}$ mice, suggesting that the *Tnks2*$^{PD\Delta neo\Delta}$ allele has a more severe effect on growth than does the *Tnks2*$^{PD\Delta}$ allele.

Normal telomere length in *Tnks2*$^{PD\Delta-/-}$ and *Tnks2*$^{PD\Delta neo\Delta-/-}$ mice. We determined whether deletion of the PARP domain of *Tnks2* affected the length of the telomeric repeats. First, we used flow-FISH, which measures the total telomere DNA content in a cell population (4, 47). We determined the average telomere fluorescence (expressed in arbitrary units) in splenocytes and thymocytes from six sets of littermate *Tnks2*$^{PD\Delta+/+}$ versus *Tnks2*$^{PD\Delta-/-}$ mice. As shown in Table 1, there was no significant difference between *Tnks2*$^{PD\Delta+/+}$ and *Tnks2*$^{PD\Delta-/-}$ mice. To analyze telomere length distributions, we performed Q-FISH (45, 62), a technique that measures the telomeric DNA signal at each chromosome end in individual metaphase cells (Fig. 4A). As shown in Fig. 4B, the telomere length distribution was similar in *Tnks2*$^{PD\Delta+/+}$ and *Tnks2*$^{PD\Delta-/-}$ splenocytes. As an alternative to fluorescence measurements, we used telomere restriction fragment analysis to measure telomere length. As shown in Fig. 4C, telomere restriction fragment analysis of primary and immortalized MEFs from *Tnks2*$^{PD\Delta+/+}$, *Tnks2*$^{PD\Delta+/-}$, and *Tnks2*$^{PD\Delta-/-}$ mice showed no differences in telomere length.

Similar telomere length analysis was performed on *Tnks2*$^{PD\Delta neo\Delta}$ mice. For flow-FISH, we determined the average telomere fluorescence in splenocytes and thymocytes from five sets of littermate *Tnks2*$^{PD\Delta neo\Delta+/+}$ (or +/−) versus *Tnks2*$^{PD\Delta neo\Delta-/-}$ mice. As shown in Table 1 there was no significant difference between *Tnks2*$^{PD\Delta neo\Delta+/+}$ (or +/−) and *Tnks2*$^{PD\Delta neo\Delta-/-}$ mice. In agreement, Q-FISH analysis (Fig. 4D) indicated that telomere length distribution was similar in *Tnks2*$^{PD\Delta neo\Delta+/+}$ and *Tnks2*$^{PD\Delta neo\Delta-/-}$ splenocytes. Together these data indicate that a catalytically PARP-active Tnks2 is not required for telomere length maintenance in mice.

Normal telomere capping in *Tnks2*$^{PD\Delta}$ and *Tnks2*$^{PD\Delta neo\Delta}$ mice. To study the effect of the *Tnks2* PARP domain deletion on telomere function, we analyzed 100 metaphase cells prepared from splenocytes from *Tnks2*$^{PD\Delta+/+}$ and *Tnks2*$^{PD\Delta-/-}$ mice by Q-FISH for chromosomal aberrations. We did not detect any change in signal free ends, end-to-end fusions, or chromosome breakage (Table 2). Similar analysis of splenocytes from *Tnks2*$^{PD\Delta neo\Delta+/+}$ and *Tnks2*$^{PD\Delta neo\Delta-/-}$ mice showed no chromosomal abnormalities (Table 2).

Telomere length is maintained during prolonged culture of *Tnks2*$^{PD\Delta-/-}$ ES cells. Previous studies have shown that, in ES cells deficient in telomerase, telomeres undergo shortening and show an increase in end-to-end fusions (37, 38, 43, 44). This phenotype is more apparent as ES cells are continually passaged. To determine if a deficiency in Tnks2 might influence telomere function during long-term growth, we generated *Tnks2*$^{PD\Delta-/-}$ ES cell clones from a G418-resistant *Tnks2*$^{PD\Delta+/-}$ ES cell clone by culture at increased G418 concentration. Clones were screened using the same PCR strategy described for Fig. 2C, and two *Tnks2*$^{PD\Delta-/-}$ ES cell clones (A3 and C10) were isolated (Fig. 5A). Immunoblot analysis indicated that (like *Tnks2*$^{PD\Delta-/-}$ mice) *Tnks2*$^{PD\Delta-/-}$ ES cells were deficient in wild-type Tnks2 protein but did express truncated (PARP-deleted) Tnks2 alone and fused to neo (Fig. 5B). We used Q-FISH to examine telomeres in *Tnks2*$^{PD\Delta+/+}$ versus *Tnks2*$^{PD\Delta-/-}$ ES cell clones. As shown in Fig. 5C and D we did not detect telomere shortening in *Tnks2*$^{PD\Delta-/-}$ ES cell clone A3 or C10 upon prolonged cell culture (from pd 42 to pd 212). In fact, the *Tnks2*$^{PD\Delta+/+}$ and the *Tnks2*$^{PD\Delta-/-}$ ES cell clones showed a slight increase in telomere length during long-term growth, as has been reported previously for wild-type ES cells (37). Note that *Tnks2*$^{PD\Delta-/-}$ ES cell clones had longer telomeres than *Tnks2*$^{PD\Delta+/+}$ ES cells even at pd 42. This is likely due to the additional pd's that the *Tnks2*$^{PD\Delta-/-}$ ES cell clones underwent during G418 selection. Regardless, all three lines showed a similar increase in telomere length over 170 pd's (WT, 28%; A3, 29%; C10, 26%), indicating that the *Tnks2* PARP domain deletion had no effect on telomere length maintenance during prolonged cell culture.

To study the effect of the *Tnks2* PARP domain deletion on telomere capping during prolonged cell culture, we analyzed 50 metaphase cells prepared from *Tnks2*$^{PD\Delta+/+}$ and *Tnks2*$^{PD\Delta-/-}$ ES cell cultures at 42 versus 212 pd's for chromosomal aberrations. We did not detect any change in signal free ends, end-to-end fusions, or chromosome breakage (Table 3).

DISCUSSION

Tankyrase 2 and telomere function in mice. We have shown here that tankyrase 2 (like its closely related homolog tankyrase 1) can act as a positive regulator of telomere length when overexpressed in human cells (Fig. 1A to C). Telomere elongation by tankyrase 2 was found to be dependent on its catalytic PARP

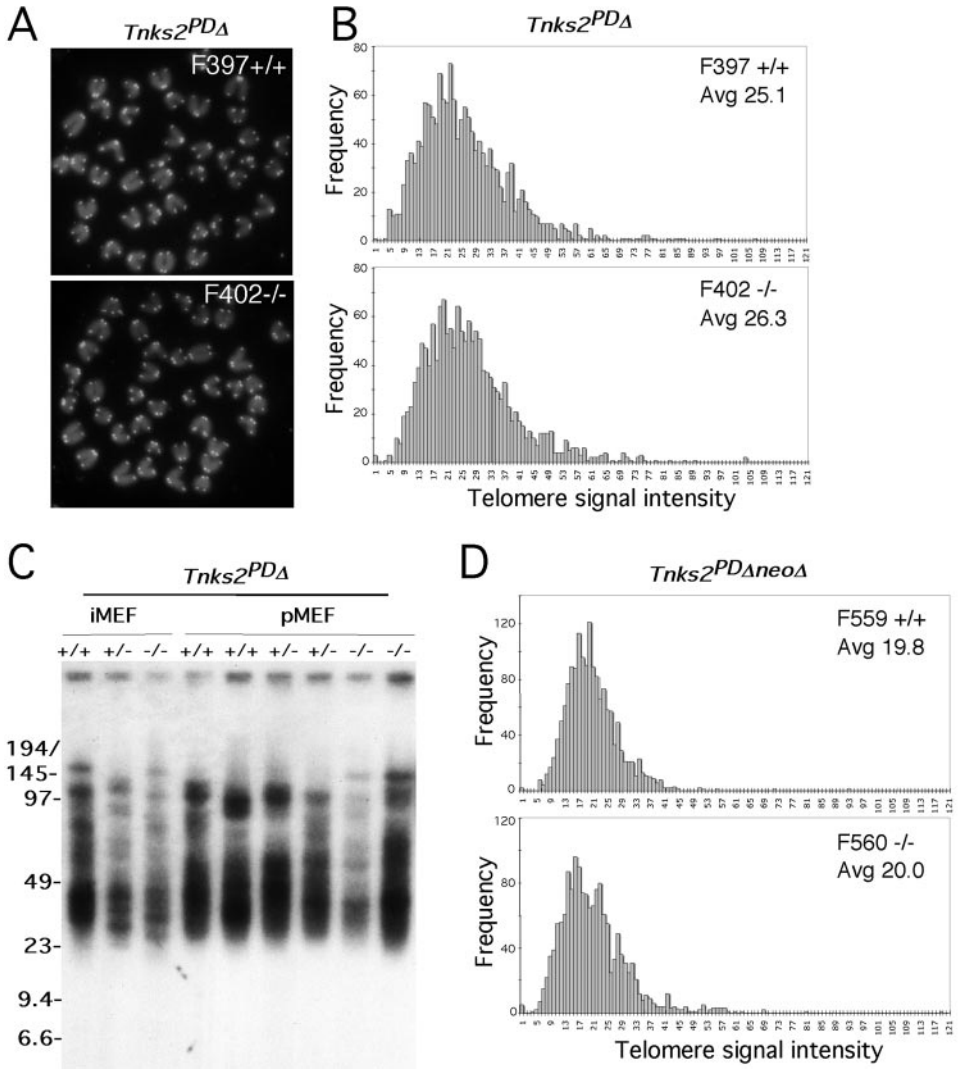

FIG. 4. Telomere length analysis of $Tnks2^{PD\Delta}$ and $Tnks2^{PD\Delta neo\Delta}$ mice. (A) Images of representative metaphase spreads from splenocytes of $Tnks2^{PD\Delta+/+}$ or $Tnks2^{PD\Delta-/-}$ mice. DNA was stained with DAPI (4′,6′-diamidino-2-phenylindole), and telomeres were stained with a Cy3-labeled PNA telomere probe. (B) Q-FISH analysis of individual metaphase preparations from splenocytes of $Tnks2^{PD\Delta+/+}$ or $Tnks2^{PD\Delta-/-}$ mice. Data were accumulated by using 10 metaphases for each histogram. The "frequency" or number of telomeres within a given range of telomeric DNA intensities was plotted against the telomere DNA signal intensity with arbitrary units (0 = no telomeric DNA signal, and increasing increments of arbitrary telomere fluorescence units up to 121). Average telomere length is indicated for each histogram. (C) Telomere restriction fragment analysis by pulsed-field gel electrophoresis of immortalized MEFs (iMEFs) or primary MEFs (pMEFs) from $Tnks2^{PD\Delta+/+}$, $Tnks2^{PD\Delta+/-}$, or $Tnks2^{PD\Delta-/-}$ mice. Numbers at left are molecular masses in kilobases. (D) Q-FISH analysis of individual metaphase preparations from splenocytes of $Tnks2^{PD\Delta neo\Delta+/+}$ or $Tnks2^{PD\Delta neo\Delta-/-}$ mice was performed as described for panel B.

TABLE 2. Analysis of chromosomal abnormalities in splenocytes of $Tnks2^{PD\Delta}$ (−/−) and $Tnks2^{PD\Delta neo\Delta}$ (−/−) mice and their wild-type (+/+) littermates

Genotype	No. of metaphases	% (no./total no. of chromosomes)		
		Signal free ends	End-to-end fusions	Chromosome breakages
$Tnks2^{PD\Delta}$ (+/+)	100	0.45 (18/3,987)	0 (0/3,987)	0 (0/3,987)
$Tnks2^{PD\Delta}$ (−/−)	100	0.40 (16/3,992)	0 (0/3,992)	0 (0/3,992)
$Tnks2^{PD\Delta neo\Delta}$ (+/+)	100	0.43 (17/3,973)	0 (0/3,973)	0.03 (1/3,973)
$Tnks2^{PD\Delta neo\Delta}$ (−/−)	100	0.48 (19/3,971)	0 (0/3,971)	0.05 (2/3,971)

activity. To determine if tankyrase 2 was required for telomere maintenance in vivo, we analyzed telomere function in mice containing a PARP domain-deleted Tnks2. Telomere length analysis using three different methods (Q-FISH, flow-FISH, and telomere restriction fragment analysis) revealed no change in telomere length in Tnks2 PARP domain-deleted mice (Fig. 4; Table 1). Moreover, Tnks2 PARP domain-deleted ES cells, which were grown for 212 pd's, showed no telomere shortening (Fig. 5). Together these data indicate that a PARP-active Tnks2 is not required for telomere length maintenance in vivo in mice and during long-term growth of mouse cells.

How can we reconcile the lack of requirement for PARP-active tankyrase 2 in telomere length maintenance in mice with

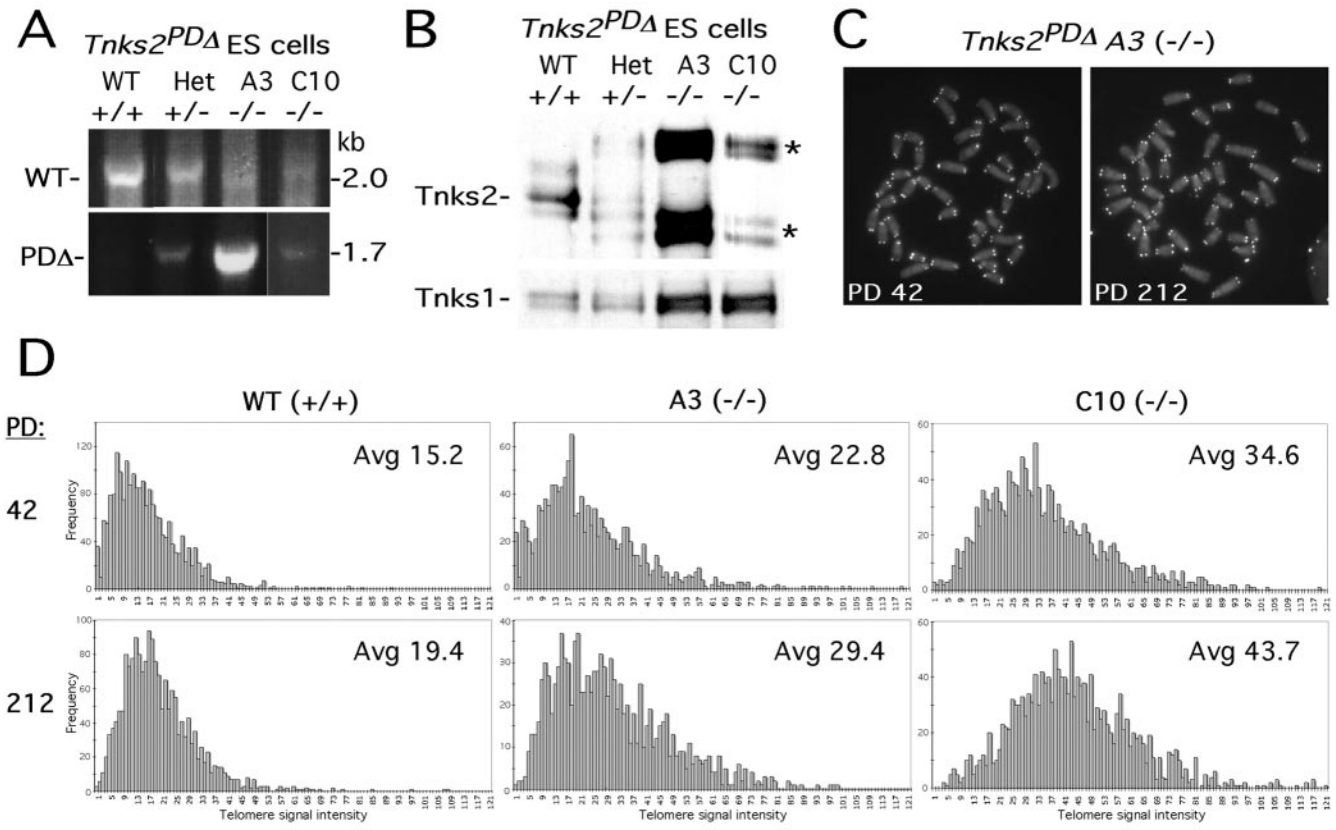

FIG. 5. Analysis of *Tnks2*$^{PD\Delta}$ ES cells. (A) PCR analysis of *Tnks2*$^{PD\Delta}$ ES cells of the indicated genotypes (+/+; +/−; and two independently isolated −/− clones, A3 and C10) using the primers indicated in Fig. 2A. (B) Immunoblot analysis of *Tnks2*$^{PD\Delta}$ ES cells of the indicated genotypes. Cell extracts were immunoprecipitated with anti-tankyrase 1 465 (detects tankyrases 1 and 2) and immunoblotted with anti-tankyrase 2 608 or anti-tankyrase 1 465 antibodies. Asterisks indicate alternative products of Tnks2 lacking the catalytic PARP domain. (C) Images of representative metaphase spreads from *Tnks2*$^{PD\Delta-/-}$ ES cells (clone A3) at pd's 42 and 212. DNA was stained with DAPI, and telomeres were stained with a Cy3-labeled PNA telomere probe. (D) Q-FISH analysis of individual metaphase preparations from *Tnks2*$^{PD\Delta+/+}$ or *Tnks2*$^{PD\Delta-/-}$ (clones A3 and C10) at pd's 42 and 212. Data were accumulated by using 10 metaphases for each histogram. The "frequency" or number of telomeres within a given range of telomeric DNA intensities was plotted against the telomere DNA signal intensity with arbitrary units (0 = no telomeric DNA signal, and increasing increments of arbitrary telomere fluorescence units up to 121). Average telomere length is indicated for each histogram.

our demonstration that a PARP-active tankyrase 2 induces telomere elongation in human cells? Our studies, showing that tankyrase 2 (or tankyrase 1) can induce telomere elongation in human cells, are based on overexpression analysis. By contrast, our studies with mice utilize deletion analysis. Thus, it is possible that, in the absence of a catalytically active Tnks2, a redundant role for Tnks1 in telomere function is revealed, i.e., Tnks1 function is sufficient to maintain telomere length in the absence of Tnks2. Ultimately, a double knockout mouse, deficient in both Tnks1 and Tnks2, will be needed to address this question.

Other PARPs and telomeres. Other PARPs besides tankyrases 1 and 2 have been suggested to play a role at telomeres.

TABLE 3. Analysis of chromosomal abnormalities in *Tnks2*$^{PD\Delta}$ (−/−) and wild-type (+/+) ES cells

Genotype	Cell line[a]	pd	No. of metaphases	No. of:		
				Signal free ends/ total chromosomes[b]	End-to-end fusions/ total chromosomes	Chromosome breakages/ total chromosomes
Tnks2$^{PD\Delta}$ (+/+)	WT	42	50	0/1,988	0/1,988	0/1,988
Tnks2$^{PD\Delta}$ (+/+)	WT	212	50	0/1,992	2/1,992	2/1,992
Tnks2$^{PD\Delta}$ (−/−)	A3	42	50	0/2,056	0/2,056	0/2,056
Tnks2$^{PD\Delta}$ (−/−)	A3	212	50	0/2,083	1/2,083	1/2,083
Tnks2$^{PD\Delta}$ (−/−)	C10	42	50	0/2,043	1/2,043	1/2,043
Tnks2$^{PD\Delta}$ (−/−)	C10	212	50	0/1,985	3/1,985	0/1,985

[a] A3 and C10 are independently derived *Tnks2*$^{PD\Delta}$ (−/−) ES cells.
[b] For detection of signal free ends, the telomere images were overexposed to intensify weak telomeric fluorescent signals.

PARP-1, the first identified member of the PARP family, is a DNA damage sensor and has also been implicated in many other cellular processes (reviewed in references 1 and 35). One report of *PARP-1*$^{-/-}$ mice showed a 30% decrease in telomere length and end-to-end fusions in 25% of cells (15), whereas another group using a different *PARP-1*$^{-/-}$ mouse found normal telomere length and chromosomal end capping (48). PARP-2, a homolog of PARP-1, has also been reported to play a role at telomeres. PARP-2 was shown to bind and poly(ADP-ribosyl)ate TRF2 (16), a telomeric DNA binding protein that has a protective function (59). *PARP-2*$^{-/-}$ cells showed normal telomere length, but an increase in chromosome/chromatid breaks and signal free ends was observed (16). Another PARP with a potential telomeric function is vault PARP (VPARP) (34). VPARP is a component of the vault complex, a large (13-MDa), highly conserved, and ubiquitously expressed ribonucleoprotein complex (reviewed in reference 60). Other components of the vault complex include major vault protein, vault RNA, and telomerase-associated protein 1 (TEP1), which binds telomerase RNA (25). Studies of *VPARP*$^{-/-}$ mice and *TEP1*$^{-/-}$ *VPARP*$^{-/-}$ mice, however, showed normal telomere length and structure (39). While it is possible that PARP-1, PARP-2, and VPARP could have functions redundant with tankyrases 1 and 2 in maintaining normal telomere length and capping of telomeres, we think it unlikely, since the only homology between these three PARPs and tankyrases 1 and 2 is in the PARP catalytic domain.

Tankyrase 2 and postnatal growth in mice. Tnks2 PARP domain-deleted mice are generated at the expected Mendelian ratios, suggesting that Tnks2 PARP activity is not required for embryonic development. Indeed, Tnks2 PARP domain-deleted neonates are indistinguishable from WT littermates from birth until postnatal day 6. However, after day 6 growth retardation becomes apparent (Fig. 3B). The Tnks2 PARP domain-deleted mice were, on average, 20% smaller than WT or heterozygous littermates (Fig. 3A, B, and D). While we do not know the mechanism for this growth defect, we speculate (based on known tankyrase 2 binding partners) that tankyrase 2 could play a role in insulin-mediated effects on postnatal growth (see below).

Thus, tankyrase 2 has been show to bind to Grb14 (40), a member of the Grb7/10/14 family of adaptors (reviewed in reference 27). Grb14 binds activated IR (30) and inhibits the phosphorylation of IR substrates (6). Overexpression of Grb14 has been shown to inhibit the activation of downstream insulin signaling cascades (6, 26, 30). Consistent with the role of Grb14 as an inhibitor of IR signaling, *Grb14*$^{-/-}$ mice display improved glucose tolerance, increased insulin sensitivity, and enhanced insulin signaling (14). Interestingly, *Grb14*$^{-/-}$ mice also exhibit decreased body mass (5 to 10%), compared to wild-type littermates (14), although this is less than the 20% that we observed in our Tnks2 PARP domain-deleted mice (Fig. 3A, B, and D). Another difference in the *Grb14*$^{-/-}$ mice is that the reduced body mass is not uniform in all tissues. Liver and spleen were significantly reduced (16% and 29%, respectively), while the heart size increased (18%) (14). This is in contrast to our Tnks2 PARP domain-deleted mice, where organ size was proportional to small body size (Fig. 3C and E). Therefore, the Tnks2-Grb14 interaction may not completely account for the small mouse phenotype.

In addition to Grb14, IRAP is another protein in the insulin pathway that has been shown to bind to tankyrase 1 or 2 and to be an acceptor of poly(ADP-ribosyl)ation (50). IRAP colocalizes with GLUT4, an insulin-responsive glucose transporter in adipocytes and muscle (46). After insulin stimulation, both IRAP and GLUT4 translocate from vesicles in the cytoplasm and trans-Golgi network to the plasma membrane (reviewed in reference 32). In *IRAP*$^{-/-}$ mice, absence of IRAP resulted in decreased GLUT4 expression (33). It has been suggested that tankyrases 1 and 2 may have a role in targeting or maintenance of GLUT4 vesicles (11, 50). Interestingly, *Glut4*$^{-/-}$ mice (similar to our Tnks2 PARP-deleted mice) display growth retardation and are 20% smaller than controls (31). However, since *IRAP*$^{-/-}$ mice do not have decreased body weight (33), the role of the IRAP-tankyrase 2 interaction in the small mouse phenotype remains to be determined.

Our studies of Tnks2 PARP domain-deleted mice have shed some light on the different functions of Tnks2 in vivo. For telomere maintenance, Tnks1 and Tnks2 could share redundant functions, but for normal postnatal growth, Tnks1 is not sufficient, as our mice display growth retardation. Further studies of these mice and of mice deficient in both Tnks1 and Tnks2 will be valuable in distinguishing the functions of Tnks1 and Tnks2 in telomere length maintenance and growth.

ACKNOWLEDGMENTS

We thank Alexandra Joyner and Frada Berenshteyn (Skirball Institute) for expert advice and assistance with ES cells and Alexandra Joyner for the targeting vector and TK-Cre mice. We thank Jasmin Dynek for generating the tankyrase 2.HE/A mutant, David Khoo for assistance with Tnks2 ES cells, and members of the Smith lab for comments on the manuscript.

S.J.H. was supported by NIH Predoctoral Training Programs (MD-PhD GM07308 and Cell and Molecular Biology GM07238). M.F.P. was supported by an Ellison Medical Foundation/AFAR Senior Postdoctoral Fellowship. Y.L. was supported by the Office of Biological and Environmental Research, U.S. Department of Energy, under contract DE-AC056-960R22464 with UT-Battelle, LLC. This work was supported by a grant from the NIH (RO1 CA95099).

REFERENCES

1. **Ame, J. C., C. Spenlehauer, and G. de Murcia.** 2004. The PARP superfamily. Bioessays **26:**882–893.
2. **Ancelin, K., M. Brunori, S. Bauwens, C. E. Koering, C. Brun, M. Ricoul, J. P. Pommier, L. Sabatier, and E. Gilson.** 2002. Targeting assay to study the *cis* functions of human telomeric proteins: evidence for inhibition of telomerase by TRF1 and for activation of telomere degradation by TRF2. Mol. Cell. Biol. **22:**3474–3487.
3. **Bae, J., J. R. Donigian, and A. J. Hsueh.** 2003. Tankyrase 1 interacts with Mcl-1 proteins and inhibits their regulation of apoptosis. J. Biol. Chem. **278:**5195–5204.
4. **Baerlocher, G. M., J. Mak, T. Tien, and P. M. Lansdorp.** 2002. Telomere length measurement by fluorescence in situ hybridization and flow cytometry: tips and pitfalls. Cytometry **47:**89–99.
5. **Bai, C. B., W. Auerbach, J. S. Lee, D. Stephen, and A. L. Joyner.** 2002. Gli2, but not Gli1, is required for initial Shh signaling and ectopic activation of the Shh pathway. Development **129:**4753–4761.
6. **Bereziat, V., A. Kasus-Jacobi, D. Perdereau, B. Cariou, J. Girard, and A. F. Burnol.** 2002. Inhibition of insulin receptor catalytic activity by the molecular adapter Grb14. J. Biol. Chem. **277:**4845–4852.
7. **Carmeliet, P., V. Ferreira, G. Breier, S. Pollefeyt, L. Kieckens, M. Gertsenstein, M. Fahrig, A. Vandenhoeck, K. Harpal, C. Eberhardt, C. Declercq, J. Pawling, L. Moons, D. Collen, W. Risau, and A. Nagy.** 1996. Abnormal blood vessel development and lethality in embryos lacking a single VEGF allele. Nature **380:**435–439.
8. **Chang, P., M. Coughlin, and T. J. Mitchison.** 2005. Tankyrase-1 polymerization of poly(ADP-ribose) is required for spindle structure and function. Nat. Cell Biol. **7:**1133–1139.
9. **Chang, W., J. N. Dynek, and S. Smith.** 2005. NuMA is a major acceptor of poly(ADP-ribosyl)ation by tankyrase 1 in mitosis. Biochem. J. **391:**177–184.

10. **Chang, W., J. N. Dynek, and S. Smith.** 2003. TRF1 is degraded by ubiquitin-mediated proteolysis after release from telomeres. Genes Dev. **17:**1328–1333.
11. **Chi, N. W., and H. F. Lodish.** 2000. Tankyrase is a golgi-associated mitogen-activated protein kinase substrate that interacts with IRAP in GLUT4 vesicles. J. Biol. Chem. **275:**38437–38444.
12. **Chong, L., B. van Steensel, D. Broccoli, H. Erdjument-Bromage, J. Hanish, P. Tempst, and T. de Lange.** 1995. A human telomeric protein. Science **270:**1663–1667.
13. **Cook, B. D., J. N. Dynek, W. Chang, G. Shostak, and S. Smith.** 2002. Role for the related poly(ADP-ribose) polymerases tankyrase 1 and 2 at human telomeres. Mol. Cell. Biol. **22:**332–342.
14. **Cooney, G. J., R. J. Lyons, A. J. Crew, T. E. Jensen, J. C. Molero, C. J. Mitchell, T. J. Biden, C. J. Ormandy, D. E. James, and R. J. Daly.** 2004. Improved glucose homeostasis and enhanced insulin signalling in Grb14-deficient mice. EMBO J. **23:**582–593.
15. **d'Adda di Fagagna, F., M. P. Hande, W. M. Tong, P. M. Lansdorp, Z. Q. Wang, and S. P. Jackson.** 1999. Functions of poly(ADP-ribose) polymerase in controlling telomere length and chromosomal stability. Nat. Genet. **23:** 76–80.
16. **Dantzer, F., M. J. Giraud-Panis, I. Jaco, J. C. Ame, I. Schultz, M. Blasco, C. E. Koering, E. Gilson, J. Menissier-de Murcia, G. de Murcia, and V. Schreiber.** 2004. Functional interaction between poly(ADP-ribose) polymerase 2 (PARP-2) and TRF2: PARP activity negatively regulates TRF2. Mol. Cell. Biol. **24:**1595–1607.
17. **de Lange, T.** 2005. Shelterin: the protein complex that shapes and safeguards human telomeres. Genes Dev. **19:**2100–2110.
18. **De Rycker, M., and C. M. Price.** 2004. Tankyrase polymerization is controlled by its sterile alpha motif and poly(ADP-ribose) polymerase domains. Mol. Cell. Biol. **24:**9802–9812.
19. **De Rycker, M., R. N. Venkatesan, C. Wei, and C. M. Price.** 2003. Vertebrate tankyrase domain structure and sterile alpha motif (SAM)-mediated multimerization. Biochem. J. **372:**87–96.
20. **Dynek, J. N., and S. Smith.** 2004. Resolution of sister telomere association is required for progression through mitosis. Science **304:**97–100.
21. **Fuchs, U., G. F. Rehkamp, R. Slany, M. Follo, and A. Borkhardt.** 2003. The formin-binding protein 17, FBP17, binds via a TNKS binding motif to tankyrase, a protein involved in telomere maintenance. FEBS Lett. **554:**10–16.
22. **Granger, M. P., W. E. Wright, and J. W. Shay.** 2002. Telomerase in cancer and aging. Crit. Rev. Oncol. Hematol. **41:**29–40.
23. **Greider, C. W., and E. H. Blackburn.** 1985. Identification of a specific telomere terminal transferase activity in Tetrahymena extracts. Cell **43:**405–413.
24. **Greider, C. W., and E. H. Blackburn.** 1987. The telomere terminal transferase of Tetrahymena is a ribonucleoprotein enzyme with two kinds of primer specificity. Cell **51:**887–898.
25. **Harrington, L., T. McPhail, V. Mar, W. Zhou, R. Oulton, M. B. Bass, I. Arruda, and M. O. Robinson.** 1997. A mammalian telomerase-associated protein. Science **275:**973–977.
26. **Hemming, R., R. Agatep, K. Badiani, K. Wyant, G. Arthur, R. D. Gietz, and B. Triggs-Raine.** 2001. Human growth factor receptor bound 14 binds the activated insulin receptor and alters the insulin-stimulated tyrosine phosphorylation levels of multiple proteins. Biochem. Cell Biol. **79:**21–32.
27. **Holt, L. J., and K. Siddle.** 2005. Grb10 and Grb14: enigmatic regulators of insulin action—and more? Biochem. J. **388:**393–406.
28. **Jacks, T., T. S. Shih, E. M. Schmitt, R. T. Bronson, A. Bernards, and R. A. Weinberg.** 1994. Tumour predisposition in mice heterozygous for a targeted mutation in Nf1. Nat. Genet. **7:**353–361.
29. **Kaminker, P. G., S. H. Kim, R. D. Taylor, Y. Zebarjadian, W. D. Funk, G. B. Morin, P. Yaswen, and J. Campisi.** 2001. TANK2, a new TRF1-associated PARP, causes rapid induction of cell death upon overexpression. J. Biol. Chem. **276:**35891–35899.
30. **Kasus-Jacobi, A., D. Perdereau, C. Auzan, E. Clauser, E. Van Obberghen, F. Mauvais-Jarvis, J. Girard, and A. F. Burnol.** 1998. Identification of the rat adapter Grb14 as an inhibitor of insulin actions. J. Biol. Chem. **273:**26026–26035.
31. **Katz, E. B., A. E. Stenbit, K. Hatton, R. DePinho, and M. J. Charron.** 1995. Cardiac and adipose tissue abnormalities but not diabetes in mice deficient in GLUT4. Nature **377:**151–155.
32. **Keller, S. R.** 2004. Role of the insulin-regulated aminopeptidase IRAP in insulin action and diabetes. Biol. Pharm. Bull. **27:**761–764.
33. **Keller, S. R., A. C. Davis, and K. B. Clairmont.** 2002. Mice deficient in the insulin-regulated membrane aminopeptidase show substantial decreases in glucose transporter GLUT4 levels but maintain normal glucose homeostasis. J. Biol. Chem. **277:**17677–17686.
34. **Kickhoefer, V. A., A. C. Siva, N. L. Kedersha, E. M. Inman, C. Ruland, M. Streuli, and L. H. Rome.** 1999. The 193-kD vault protein, VPARP, is a novel poly(ADP-ribose) polymerase. J. Cell Biol. **146:**917–928.
35. **Kim, M. Y., T. Zhang, and W. L. Kraus.** 2005. Poly(ADP-ribosyl)ation by PARP-1: 'PAR-laying' NAD^+ into a nuclear signal. Genes Dev. **19:**1951–1967.
36. **Kuimov, A. N., D. V. Kuprash, V. N. Petrov, K. K. Vdovichenko, M. J. Scanlan, C. V. Jongeneel, M. A. Lagarkova, and S. A. Nedospasov.** 2001. Cloning and characterization of TNKL, a member of tankyrase gene family. Genes Immun. **2:**52–55.
37. **Liu, Y., H. Kha, M. Ungrin, M. O. Robinson, and L. Harrington.** 2002. Preferential maintenance of critically short telomeres in mammalian cells heterozygous for mTert. Proc. Natl. Acad. Sci. USA **99:**3597–3602.
38. **Liu, Y., B. E. Snow, M. P. Hande, D. Yeung, N. J. Erdmann, A. Wakeham, A. Itie, D. P. Siderovski, P. M. Lansdorp, M. O. Robinson, and L. Harrington.** 2000. The telomerase reverse transcriptase is limiting and necessary for telomerase function in vivo. Curr. Biol. **10:**1459–1462.
39. **Liu, Y., B. E. Snow, V. A. Kickhoefer, N. Erdmann, W. Zhou, A. Wakeham, M. Gomez, L. H. Rome, and L. Harrington.** 2004. Vault poly(ADP-ribose) polymerase is associated with mammalian telomerase and is dispensable for telomerase function and vault structure in vivo. Mol. Cell. Biol. **24:**5314–5323.
40. **Lyons, R. J., R. Deane, D. K. Lynch, Z. S. Ye, G. M. Sanderson, H. J. Eyre, G. R. Sutherland, and R. J. Daly.** 2001. Identification of a novel human tankyrase through its interaction with the adaptor protein Grb14. J. Biol. Chem. **276:**17172–17180.
41. **Maser, R. S., and R. A. DePinho.** 2002. Connecting chromosomes, crisis, and cancer. Science **297:**565–569.
42. **Monz, D., A. Munnia, N. Comtesse, U. Fischer, W. I. Steudel, W. Feiden, B. Glass, and E. U. Meese.** 2001. Novel tankyrase-related gene detected with meningioma-specific sera. Clin. Cancer Res. **7:**113–119.
43. **Niida, H., T. Matsumoto, H. Satoh, M. Shiwa, Y. Tokutake, Y. Furuichi, and Y. Shinkai.** 1998. Severe growth defect in mouse cells lacking the telomerase RNA component. Nat. Genet. **19:**203–206.
44. **Niida, H., Y. Shinkai, M. P. Hande, T. Matsumoto, S. Takehara, M. Tachibana, M. Oshimura, P. M. Lansdorp, and Y. Furuichi.** 2000. Telomere maintenance in telomerase-deficient mouse embryonic stem cells: characterization of an amplified telomeric DNA. Mol. Cell. Biol. **20:**4115–4127.
45. **Poon, S. S., U. M. Martens, R. K. Ward, and P. M. Lansdorp.** 1999. Telomere length measurements using digital fluorescence microscopy. Cytometry **36:**267–278.
46. **Ross, S. A., H. M. Scott, N. J. Morris, W. Y. Leung, F. Mao, G. E. Lienhard, and S. R. Keller.** 1996. Characterization of the insulin-regulated membrane aminopeptidase in 3T3-L1 adipocytes. J. Biol. Chem. **271:**3328–3332.
47. **Rufer, N., W. Dragowska, G. Thornbury, E. Roosnek, and P. M. Lansdorp.** 1998. Telomere length dynamics in human lymphocyte subpopulations measured by flow cytometry. Nat. Biotechnol. **16:**743–747.
48. **Samper, E., F. A. Goytisolo, J. Menissier-de Murcia, E. Gonzalez-Suarez, J. C. Cigudosa, G. de Murcia, and M. A. Blasco.** 2001. Normal telomere length and chromosomal end capping in poly(ADP-ribose) polymerase-deficient mice and primary cells despite increased chromosomal instability. J. Cell Biol. **154:**49–60.
49. **Sbodio, J. I., and N. W. Chi.** 2002. Identification of a tankyrase-binding motif shared by IRAP, TAB182, and human TRF1 but not mouse TRF1. NuMA contains this RXXPDG motif and is a novel tankyrase partner. J. Biol. Chem. **277:**31887–31892.
50. **Sbodio, J. I., H. F. Lodish, and N. W. Chi.** 2002. Tankyrase-2 oligomerizes with tankyrase-1 and binds to both TRF1 (telomere-repeat-binding factor 1) and IRAP (insulin-responsive aminopeptidase). Biochem. J. **361:**451–459.
51. **Seimiya, H., and S. Smith.** 2002. The telomeric poly(ADP-ribose) polymerase, tankyrase 1, contains multiple binding sites for telomeric repeat binding factor 1 (TRF1) and a novel acceptor, 182-kDa tankyrase-binding protein (TAB182). J. Biol. Chem. **277:**14116–14126.
52. **Smith, S.** 2001. The world according to PARP. Trends Biochem. Sci. **26:** 174–179.
53. **Smith, S., and T. de Lange.** 1999. Cell cycle dependent localization of the telomeric PARP, tankyrase, to nuclear pore complexes and centrosomes. J. Cell Sci. **112:**3649–3656.
54. **Smith, S., and T. de Lange.** 2000. Tankyrase promotes telomere elongation in human cells. Curr. Biol. **10:**1299–1302.
55. **Smith, S., I. Giriat, A. Schmitt, and T. de Lange.** 1998. Tankyrase, a poly-(ADP-ribose) polymerase at human telomeres. Science **282:**1484–1487.
56. **Smorgorzewska, A., and T. de Lange.** 2004. Regulation of telomerase by telomeric proteins. Annu. Rev. Biochem. **73:**177–208.
57. **Todaro, G. J., and H. Green.** 1963. Quantitative studies of the growth of mouse embryo cells in culture and their development into established lines. J. Cell Biol. **17:**299–313.
58. **van Steensel, B., and T. de Lange.** 1997. Control of telomere length by the human telomeric protein TRF1. Nature **385:**740–743.
59. **van Steensel, B., A. Smogorzewska, and T. de Lange.** 1998. TRF2 protects human telomeres from end-to-end fusions. Cell **92:**401–413.
60. **van Zon, A., M. H. Mossink, R. J. Scheper, P. Sonneveld, and E. A. Wiemer.** 2003. The vault complex. Cell Mol. Life Sci. **60:**1828–1837.
61. **Wang, Y., N. Erdmann, R. J. Giannone, J. Wu, M. Gomez, and Y. Liu.** 2005. An increase in telomere sister chromatid exchange in murine embryonic stem cells possessing critically shortened telomeres. Proc. Natl. Acad. Sci. USA **102:**10256–10260.
62. **Zijlmans, J. M., U. M. Martens, S. S. Poon, A. K. Raap, H. J. Tanke, R. K. Ward, and P. M. Lansdorp.** 1997. Telomeres in the mouse have large inter-chromosomal variations in the number of T2AG3 repeats. Proc. Natl. Acad. Sci. USA **94:**7423–7428.